IOP Publishing Journal of Physics D: Applied Physics

J. Phys. D: Appl. Phys. **54** (2021) 295001 (9pp) https://doi.org/10.1088/1361-6463/abfb1c

Vector magneto-optical magnetometer based on resonant all-dielectric gratings with highly anisotropic iron garnet films

Daria O Ignatyeva[1,2,3,*], Grigory A Knyazev[1,3], Andrey N Kalish[1,3,4,*], Alexander I Chernov[1,4,5] and Vladimir I Belotelov[1,2,3]

[1] Russian Quantum Center, Skolkovo Innovation City, Moscow 121353, Russia
[2] Vernadsky Crimean Federal University, Simferopol 295007, Russia
[3] Faculty of Physics, Lomonosov Moscow State University, Moscow 119991, Russia
[4] NTI Center for Quantum Communications, National University of Science and Technology MISiS, Moscow 119049, Russia
[5] Center for Photonics and 2D Materials, Moscow Institute of Physics and Technology, National Research University, Dolgoprudny 141700, Russia

E-mail: ignatyeva@physics.msu.ru and kalish@physics.msu.ru

Received 8 February 2021, revised 6 April 2021
Accepted for publication 23 April 2021
Published 13 May 2021

Abstract

Sensitive vector magnetometry with high spatial resolution is important for various practical applications, such as magnetocardiography, magnetoencephalography, explosive materials detection and many others. We propose a magnetometer based on magnetic iron garnet film possessing a very high magnetic anisotropy, placed in a rotating external magnetic field. Each of the measured magnetic field spatial components produces different temporal harmonics in the out-of-plane magnetization dependence. Our analysis based on numerical simulation shows that the dielectric resonant grating placed on the top of an ultrathin film enhanced the magneto-optical (MO) response by ten times. It allows one to reduce the thickness of the film, which makes it possible to achieve several times higher spatial resolution in the perpendicular to the film direction, up to 30 nm. The reported MO magnetometer allows one to measure simultaneously all three spatial components of the magnetic field with high spatial resolution and sensitivity up to 100 pT Hz$^{-1/2}$.

Keywords: magnetic field sensors, all-dielectric nanophotonics, magnetic anisotropy, ultrathin magnetic films

(Some figures may appear in color only in the online journal)

1. Introduction

Registration of weak magnetic fields is an important approach for study of different animate and inanimate objects. Magnetocardiography based on the measurement of the magnetic signals associated with the blood currents provides novel information essential for diagnostics [1, 2]. Detection of weak magnetic signals is important, for example, for magnetoencephalography [3], sensing of explosive materials [4], particle physics [5].

For many practical applications, it is essential to provide not only high sensitivity of the magnetometer, but also micrometer

[*] Authors to whom any correspondence should be addressed.

spatial resolution and an ability to distinguish orientation of the external magnetic field. There are many types of magnetometers that have been developed nowadays, among which one of the most promising approaches is flux-gate magnetometry [6–9] reaching a 100 fT Hz$^{-1/2}$ sensitivity [9] in a wide frequency range up to GHz frequencies. The flux-gate magnetometry is based on the measurement of the medium magnetization under the impact of the external magnetic field. It was recently shown that contactless magneto-optical (MO) reading of the magnetization state allows one to measure magnetic fields in vector format [10, 11] with micrometer spatial resolution [12]. Therefore, the enhancement of the MO effects is a vital problem of the flux-gate magnetometry.

Recently various nanostructures were demonstrated to enhance the MO effects, including photonic crystal-based [13–16], nanoplasmonic [17–19] and all-dielectric ones [20–23]. Due to the low optical losses and simplicity of fabrication and measurements, all-dielectric nanostructured films seem to be one of the most promising.

Other approaches to magnetometry include superconducting quantum interference devices (SQUIDs) [24], surface acoustic waves [25], nitrogen-vacancy (NV) centers in diamond [26], planar Hall effect [27], and optical fibers with magnetic fluids [28]. However, in most cases they do not provide 3D vector magnetometry with high sensitivity. For example, sensors based on NV-centers in diamond allow measurement of all vector components of magnetic field but with sensitivity of about several nT Hz$^{-1/2}$ and the detection volume is as large as 1 μm [26]. SQUID magnetometers provide outstanding sensitivity, about 0.1 pT, but operate only at cryogenic temperatures. The problem of simultaneous high sensitivity, compactness, detection of all three components of magnetic field and operation at room temperatures is of vital importance and for that goal we propose to apply flux-gate magnetometry with MO reading.

We consider a 1D TiO_2 grating deposited on the top of the smooth ultrathin iron garnet film grown on a gadolinium-gallium garnet (GGG) substrate and having a very high magnetic anisotropy. Performed analysis and numerical simulations show that one can perform vector magnetometry in the proposed structure with a high sensitivity up to 100 pT for Hz bandwidth. The subwavelength size of grating perforation and film width provides the significant device miniaturization. Moreover, the magnetic film thickness determines the spatial resolution of the magnetometer which is 30 nm in the reported device.

In this work, we demonstrate an approach for one order increase of sensitivity for both in-plane and perpendicular directions together with an increase of spatial resolution. The main component that provides the enhancement is the dielectric grating placed on a thin magnetic film. We show that the high magnetic anisotropy of films, which is often undesirable for magnetic sensors fabrication because of non-uniform rotation of magnetization vector, can be used to simultaneously measure all components of the magnetic field due to application of optical readout.

2. Dynamics of magnetization in magnetic film with strong anisotropy

Let us consider a magnetic dielectric film of cubic crystal lattice and crystallographic axis orientation (111) placed into an external saturating magnetic field **H** (see figures 1(a) and (b)) that uniformly rotates in the film plane with a frequency ω. The examined problem also contains a weak measurable field $\mathbf{h} \ll \mathbf{H}$ with an arbitrary direction and thus having arbitrary $\mathbf{h} = \{h_x, h_y, h_z\}$ spatial components. We consider an iron garnet film with high cubic magnetic anisotropy, for example $(Bi_{1.1}Lu_{1.45}Pr_{0.2}Tm_{0.2}Gd_{0.05})(Fe_{3.5}Al_{0.8}Ga_{0.7})O_{12}$ [10] or $Tm_3Fe_{4.3}Sc_{0.7}O_{12}$ [29]. Due to high anisotropy the dynamics of the magnetization **M** vector under the **H** impact is rather complicated in such films and, moreover, **M** direction does not coincide with **H** even in the quasi-static case ($\omega \ll \gamma H$). Let us now discuss how this peculiar dynamics gives rise to the 3D magnetometry and allows the film magnetization to be sensitive to all of the **h** spatial components.

The condition for the minimum free energy of a magnetic film gives the following expressions for the out-of-plane angle θ and azimuthal angle φ (see figure 1(b)) that determine the direction of the magnetization in the quasi-static case [10]:

$$\theta = \frac{\frac{\sqrt{2}}{3} K_1 \sin\left(3\left(\varphi - \varphi_K\right)\right) + h_z M_s}{4\pi M_s^2 - 2K_U - K_1 + HM_s \cos\left(\varphi - \varphi_H\right) + M_s h_x \cos\varphi + M_s h_y \sin\varphi}, \tag{1}$$

$$M_s h_x \sin\varphi - M_s h_y \cos\varphi + HM_s \sin\left(\varphi - \varphi_H\right) - \sqrt{2}\theta K_1 \cos\left(3\left(\varphi - \varphi_K\right)\right) = 0, \tag{2}$$

where φ_K is the angle between the anisotropy axis $[2\bar{1}\bar{1}]$ and the axis X, φ_H is the angle between **H** and X, K_1 is the cubic anisotropy constant, K_U is the uniaxial anisotropy constant (see figure 1(b) scheme). The analytical description is performed for arbitrary values of φ_K, while in numerical simulations $\varphi_K = 0$ for the definiteness.

Since we consider a rotating magnetic field, the following condition describes magnetic field direction:

$$\varphi_H = \omega t + \varphi_K, \tag{3}$$

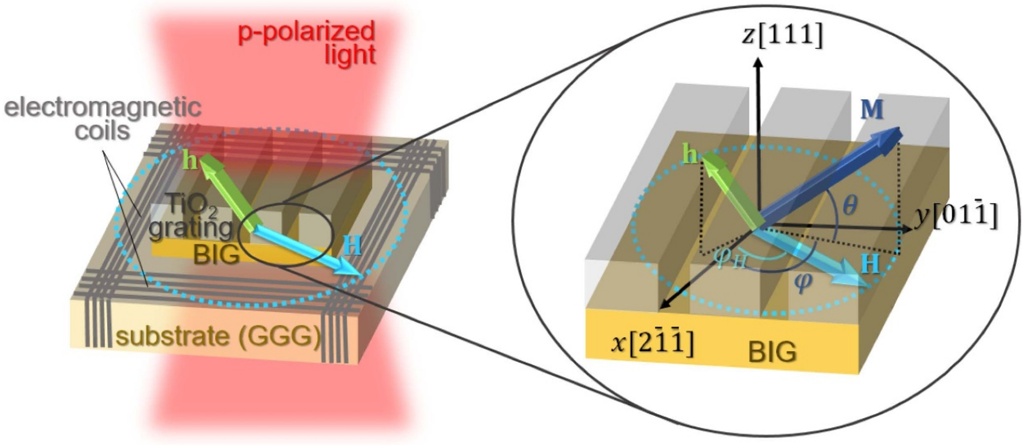

(a) (b)

Figure 1. 1D grating-based magneto-optical vector magnetometer. (a) Device principal scheme. (b) Magnetization **M** motion in the iron garnet film with high magnetic anisotropy under the action of the rotating magnetic field **H.**

$$|H| = \text{const.} \tag{4}$$

Analysis shows that under the assumption that the measured field is small ($H \gg h$) we can obtain the following equations for θ and φ:

$$\theta = \frac{K}{A}\left(\frac{1}{3}\sin(3\omega t) + \frac{h_y}{2H}\left(\cos(4\omega t + \varphi_\mathrm{K}) + \cos(2\omega t - \varphi_\mathrm{K})\right) + \frac{h_x}{2H}\left(\sin(2\omega t - \varphi_\mathrm{K}) - \sin(4\omega t + \varphi_\mathrm{K})\right) + \frac{h_z K}{2HA}\left(1 + \cos(6\omega t)\right)\right), \tag{5}$$

$$\varphi = \frac{h_y \cos(\omega t + \varphi_\mathrm{K}) - h_x \sin(\omega t + \varphi_\mathrm{K}) + \frac{K^2}{6A}\sin(6\omega t) + \frac{h_z K}{A}\cos(3\omega t)}{H} + \omega t + \varphi_\mathrm{K}. \tag{6}$$

In equations (5) and (6), we use the following designations:

$$A = 4\pi M_\mathrm{s} - \frac{2K_\mathrm{U}}{M_\mathrm{s}} - \frac{K_1}{M_\mathrm{s}} + H,$$
$$K = \frac{\sqrt{2}K_1}{M_\mathrm{s}}. \tag{7}$$

Here we also assume that $\frac{K^2}{A} \ll H \ll K$, which provides that $|\varphi - \varphi_\mathrm{H}| \ll 1$. The Fourier spectra of the MO signal associated with $\theta(t)$ determined by equation (5) provides different temporal harmonics corresponding to the external and measured magnetic field components:

$$\theta_{3\omega} = \frac{K}{3A}\sin(3\omega t),$$
$$\theta_{4\omega} = \frac{K}{2AH}h_\tau \cos(4\omega t + \varphi_\mathrm{K} + \varphi_\mathrm{h}),$$
$$\theta_{2\omega} = \frac{K}{2AH}h_\tau \cos(2\omega t - \varphi_\mathrm{K} - \varphi_\mathrm{h}),$$
$$\theta_{6\omega} = \frac{K}{2AH}h_z \cos(6\omega t) \tag{8}$$

where $h_\tau = \sqrt{h_x^2 + h_y^2}$, and $\varphi_\mathrm{h} = \tan^{-1}\frac{h_y}{h_x}$. Therefore, according to equation (8), measurement of only $\theta(t)$ dependence is enough to determine both in-plane and out-of-plane components of the weak magnetic field **h** via the magnitudes and the phases of the corresponding harmonics. Note that all harmonics in equation (8) are proportional to K, so they arise solely due to magnetic anisotropy of the film. Typical values of $K = 6.7$ Oe and $A = 1.6 \times 10^3$ Oe [29] in the iron garnets produce rather small values of $\theta_{3\omega} \approx 0.01$. Therefore, amplification of the observed θ-associated MO signal is important for the increase of the magnetometer sensitivity. Taking thicker iron garnet films [10] allows one to increase the Faraday rotation angle, but simultaneously lowers the spatial resolution in z-direction. We propose an alternative approach based on the fabrication of the non-magnetic nanostructure on the top of an ultrathin iron garnet film that amplifies the MO response due to the excitation of the optical resonances. The essential point is utilizing ultrathin films leading to miniaturization and high spatial resolution in z-direction that can be estimated as equal to their thickness.

3. MO magnetic field sensing in 1D gratings

Magneto-optics is a very convenient tool for measurement of the out-of-plane magnetization component of the iron garnet film, which contains the information on both in-plane and out-of-plane components of the measured weak magnetic field. There are two MO effects, the polarization Faraday rotation and the even MO intensity modulation, which arise from the M_z component and should be taken into account. Both of these effects can be significantly enhanced in nanostructures with guided modes [22, 23, 30] formed on the top of a thin magnetic film. This enhancement is spectrally close to the transmittance gap corresponding to the guided mode excitation. Therefore, for possible practical applications, one should bear in mind also the MO figure of merit (MO FOM) determined as MO FOM $= 0.1 \cdot \log 10 \cdot \left(\Phi/\log T^{-1}\right)$ (deg dB^{-1}), where T is transmittance, Φ is the Faraday rotation. Enhancement of the magnetometer sensitivity is realized by the increase of the signal to noise ratio. The detected signal is determined by the Φ and the noise is determined by the fluctuations of the laser intensity transmitted through the structure and characterized by the $\sqrt{\Delta T/T}$ magnitude [10]. Therefore, a value of the MO signal determined as MO signal $= \Phi\sqrt{T}$ will also be considered further.

In contrast to [22, 23, 30], here we focus our attention a non-magnetic grating made of TiO_2 material which refractive index $n_{TiO_2} \approx 2.45$ is close to the refractive index of the smooth ultrathin iron garnet film ($n_{BIG} = 2.53 + 0.004i$ at 780 nm wavelength [30]). The whole system of grating + magnetic film serves as a guiding layer, so due to the presence of a high-refractive index grating the resonance is observed even for an ultrathin magnetic films. The total thickness of the grating + magnetic film material is high, so the dispersions of the TE and TM modes are very close to each other. Simultaneous excitation of them results in a resonant enhancement of the Faraday rotation observed in the whole system.

We have tuned the parameters of the structure to make resonance wavelength λ correspond to the typical wavelength of laser diode: 1D TiO_2 grating having period $P = 370$ nm, TiO_2 stripe width $W = 335$ nm and height $d_{gr} = 240$ nm on an ultrathin iron garnet film with thickness $d_{BIG} = 30$ nm grown on a GGG substrate is studied. Such 1D grating is resonant, which means that no propagating diffraction orders in the reflectance or the transmittance are generated. On the other hand, it has a narrow resonance at $\lambda = 783$ nm corresponding to a guided mode excited in the hybrid iron garnet + TiO_2 grating layer. The exact resonance position for light incident normally is determined by the period of the grating $\lambda_{res} = n_\beta P$ [22] and the guided mode effective refractive index n_β which, in its turn, depends on the parameters of the structure including the thickness of the iron garnet film as shown in figure 2(a).

Ultrathin iron garnet films support excitation of the guided modes with the efficiencies comparable to the thicker films up to 100 nm thickness (see figures 2(a) and (b)), however the produced Faraday rotation is rather small. With the growth of the film thickness, Faraday rotation simultaneously increases, at the same time the transmittance gets reduced, so that the value of the MO signal is almost saturated for the films thicker than 30 nm. Therefore, we choose a 30 nm thick BIG film to demonstrate the advantages of the proposed approach for the ultrathin magnetic films.

The optical transmittance spectra and the spectra of the Faraday rotation angle for a smooth iron garnet film and the considered heterostructure with resonant grating are shown in figure 2(c). Notice a two orders enhancement of the Faraday rotation angle compared to the smooth film exhibiting Faraday rotation equal to $\Phi = 0.04°$. This enhancement is due to the excitation of the TM_0 mode by the incident p-polarized light (see H_y and E_x electromagnetic field distributions shown in figures 3(b) and (d)). The magnetization of the film results in the conversion of the polarization and excitation of the TE_0 mode, which leads to the resonant enhancement of the E_y components generated by the Faraday effect. Figure 3 illustrates this process: figure 3(c) shows the distribution of E_y under the s-polarized excitation and figure 3(e) corresponds to the p-polarized excitation and conversion to the TE mode.

Let us also notice that because of utilizing dielectric grating with low optical losses the optical resonance in the examined structure is very narrow: its spectral width is $\Delta\lambda = 6.5$ nm. The resonance of the MO Faraday rotation is about 2.5 times narrower (see figure 2(d)). In order to take into account, on the one hand, very sharp resonances, and on the other hand, the finite spectral width of the light source, we performed an averaging of the values T, Φ, MO FOM, MO signal over the finite bandwidth ($\Delta\lambda_{av} = 0.2$ nm was taken as the typical spectral width of the laser diode radiation). Such consideration did not significantly affect the MO characteristics of the structure.

MO FOM and MO signal were calculated for the considered structure. Figure 2(e) shows that in spite of the transmittance decrease, both quantities in the considered nanostructure are more than one order higher than in a smooth uncoated film. Indeed, for a wavelength $\lambda = 782.5$ nm the transmittance is $T = 5\%$, the Faraday rotation is $\Phi = 1.6$ deg so the MO FOM $= 0.1$ deg dB^{-1} and MO signal $= 0.16$ deg are more than ten times higher than MO FOM $= 0.016$ deg dB^{-1} and MO signal $= 0.009$ deg values for the smooth uncoated film.

The Faraday polarization rotation Φ of the transmitted light is directly proportional to the out-of-plane magnetization component determined by the value $M_z \propto \sin\theta \approx \theta$. One may assume $\Phi = \Phi_0\theta$ where Φ_0 is the Faraday rotation angle corresponding to the sample magnetized up to saturation $M_z = M_s$ and $\theta(t)$ is determined by equation (5). The weak magnetic field $\mathbf{h}$ and external field $\mathbf{H}$ components could be measured from the following harmonics of $\Phi(t)$:

$$\begin{aligned}
\Phi_H &= \Phi_0 \frac{K}{3A} \sin(3\omega t), \\
\Phi_\tau &= \Phi_0 h_\tau \frac{K}{2AH} \left(\cos(4\omega t + \varphi_K + \varphi_h) \right. \\
&\quad \left. + \cos(2\omega t - \varphi_K - \varphi_h)\right), \\
\Phi_z &= \Phi_0 \frac{K}{2AH} h_z \cos(6\omega t),
\end{aligned} \tag{9}$$

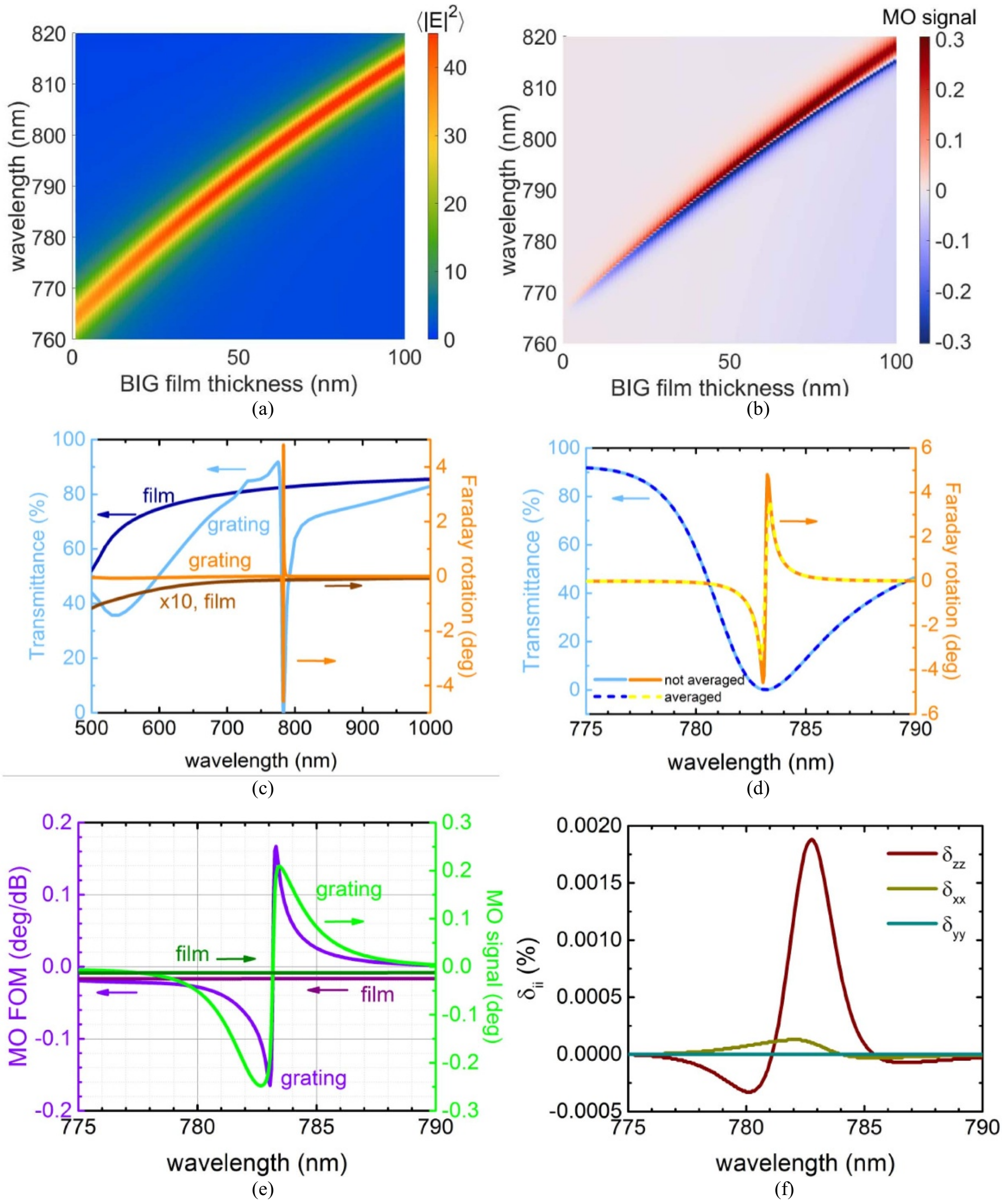

Figure 2. Calculated optical and magneto-optical spectra of the 1D resonant iron garnet $+TiO_2$ grating. (a) Spectra of the average E^2 value for the magnetic films of different thicknesses. (b) Spectra of the MO signal observed in the structures with magnetic films of different thicknesses. (c) Spectra of the transmittance (blue) and the Faraday rotation (orange) of the uncoated iron garnet film (dark lines) vs spectra of the iron garnet film with a dielectric grating (light lines), see parameters in the text. (d) Spectra of the transmittance (blue) and the Faraday rotation (orange) in the magnified wavelength scale: (solid lines) calculated for a certain λ (dashed lines) averaged over $\Delta\lambda_{\mathrm{avg}} = 0.2$ nm. (e) MO FOM (violet) and MO signal (green) of the uncoated iron garnet film (dark lines) vs spectra of the iron garnet film with a dielectric grating (bright lines), averaged over $\Delta\lambda_{\mathrm{avg}} = 0.2$ nm bandwidth. (f) Transmittance modulation coefficients δ_{ii} calculated for the considered structure.

so that the signal at the frequency 3ω corresponds to the applied magnetic field, the signal at 2ω and 4ω to the in-plane component of the measured magnetic field, and the signal at 6ω is responsible for the out-of-plane component of the measured magnetic field. The phase of the signal at 2ω and 4ω frequencies carries the information on the in-plane direction of the measured magnetic field φ_{h}.

Figure 4 illustrates the different contributions of the in-plane and out-of-plane components in the $\theta(t)$ temporal dependence and the numerically simulated optical Faraday rotation in 1D grating.

Symmetry of the structure prohibits [31] other odd intensity magnetization effects at normal incidence. However, even MO effects can arise resulting in the transmittance modulation that is quadratic on the magnetization components. Generally, at normal incidence of light the transmittance of the magnetic structure can be described as:

$$T = T_0 + \delta_{xx} m_x^2 + \delta_{yy} m_y^2 + \delta_{zz} m_z^2, \tag{10}$$

where coefficients δ_{jj} refer to the even MO effect produced by the corresponding $m_j = M_j/M_{\mathrm{s}}$ components. Formally,

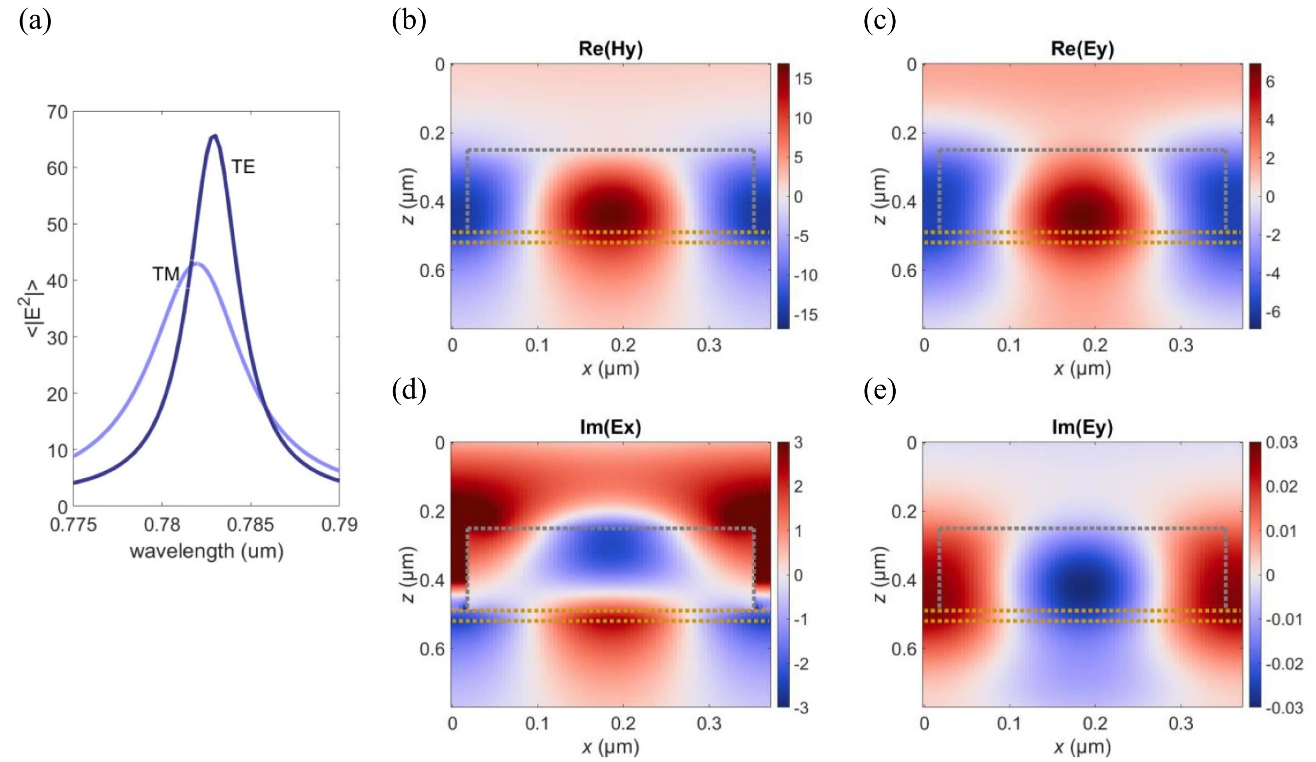

Figure 3. Mode conversion in 1D grating with a magnetic layer. (a) Average $|E|^2$ value in a magnetic film for p- and s-polarized incident light exciting TM and TE modes, correspondingly. (b)–(d) Spatial distributions of the corresponding components of the electromagnetic field for 783.4 nm wavelength and (b), (d), (e) p-polarization of the light; (c) s-polarization of the light. Electromagnetic field components were normalized on the absolute value of the incident electric field $|E_{\mathrm{inc}}|$.

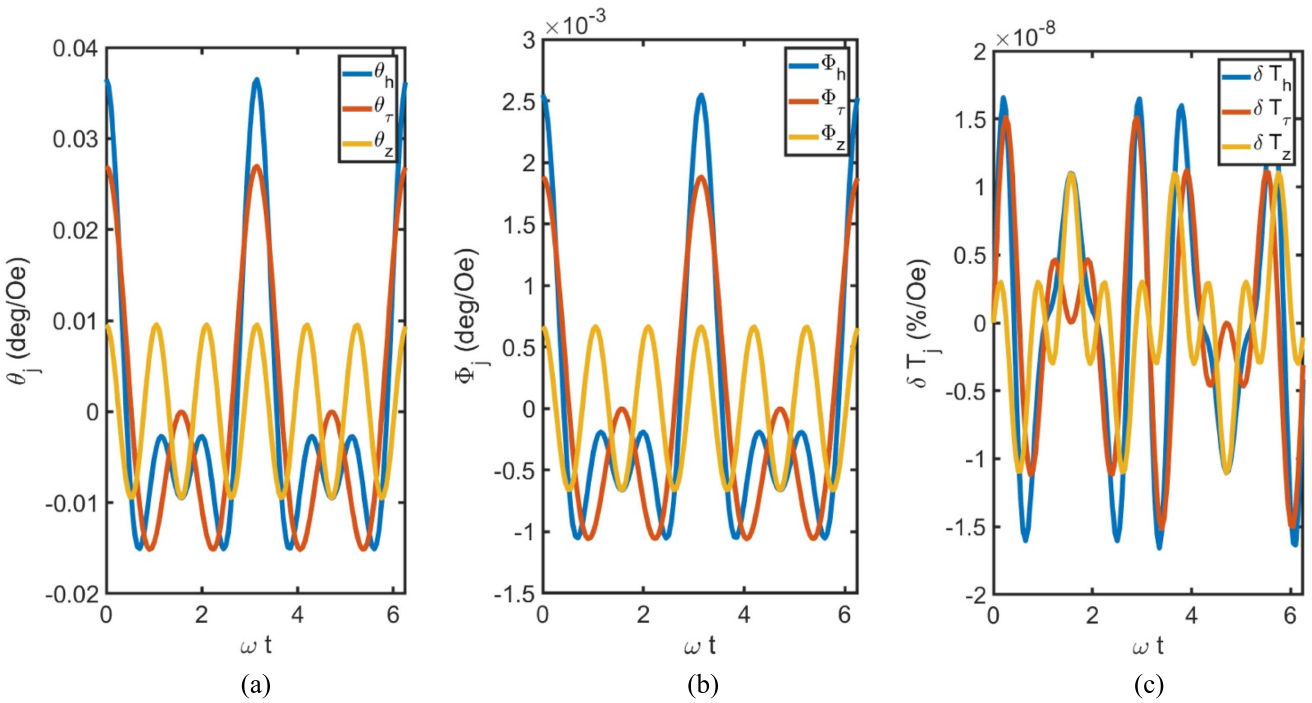

Figure 4. Contributions of the in-plane and out-of-plane **h** components to the value of (a) θ angle, (b) Faraday rotation, (c) transmittance of the structure at $\lambda = 782.5$ nm and normal incidence with magnetization determined directly by equation (5).

cross-components $\delta_{i\neq j}m_im_j$ should also be present in equation (10), however the numerical calculations show that they have several orders lower values than all the other components in both smooth and perforated films. Equation (10) can be understood in a sense of the Voigt effect for $m_{x,y}$ components: as the magnetic birefringence arises [32], it results in a small quadratic modification of the Fresnel coefficients leading to the MO variation of transmittance. The same explanation is valid for the m_z component: as the refractive index of the mode acquires MO variations, the Fresnel coefficients are modified, too.

The ratio between δ_{jj} coefficients depends on the MO properties of the structure. For a smooth iron garnet film of 30 nm thickness the coefficients are $\delta_{xx} = 3\times 10^{-7}\%, \delta_{yy} = 0, \delta_{zz} = 3\times 10^{-6}\%$. Figure 2(e) shows that in the considered nanostructure these coefficients are also small, therefore when compared to the Faraday rotation the even in magnetization impact can be neglected. However, for the nanostructured materials the ratio between these components significantly varies depending on the type of the structure, character of the modes excited in it and other parameters. For example, in several previous studies [30, 32] the plasmonic structure with iron garnet was designed with δ_{yy} that prevailed over all other coefficients. Let us analyze the situation where the δ_{zz} is higher and only the intensity of the transmitted light is measured.

As we are interested in measurement of all three orthogonal components of the weak magnetic field **h,** which are present in θ temporal dependence as harmonics with different frequencies, let us consider the nanostructure with $\delta_{zz} \gg \delta_{xx}, \delta_{yy}$, which is fulfilled for the considered nanostructure, too. Therefore, only this term in equation (11) can be considered further. The temporal dependence of the m_z could be treated as $m_z \approx \theta(t) = \theta_{\mathrm{H}}(t) + \theta_{\mathrm{h}}(t)$, where $\theta_{\mathrm{H}} \gg \theta_{\mathrm{h}}$ are the contributions corresponding to the external magnetic field **H** and the measured **h** in the temporal dependence of θ (see equation (5)). Therefore, the transmittance of the structure will experience the following temporal modulation:

$$T = T_0 + \delta_{zz}\left(\theta_{\mathrm{H}}^2 + 2\theta_{\mathrm{H}}\theta_{\mathrm{h}}\right), \tag{11}$$

and according to equation (8), the measured magnetic field **h** will be responsible for the following transmittance modulation:

$$\begin{aligned} T_\tau = {} & h_\tau \frac{K^2}{6A^2H}\delta_{zz}\sin(7\omega t + \varphi_{\mathrm{K}} + \varphi_{\mathrm{h}}) \\ & + h_\tau \frac{K^2}{6A^2H}\delta_{zz}\sin(5\omega t - \varphi_{\mathrm{K}} - \varphi_{\mathrm{h}}), \end{aligned} \tag{12}$$

$$T_\perp = h_z \frac{K^2}{6A^2H}\delta_{zz}\sin(9\omega t) - h_z \frac{K^2}{6A^2H}\delta_{zz}\sin(3\omega t), \tag{13}$$

while the applied external magnetic field **H** will result in modulation at a different frequency

$$T_{\mathrm{H}} = \frac{K^2}{18A^2}\delta_{zz}\left(1 - \cos(6\omega t)\right). \tag{14}$$

Therefore, Fourier transform of the transmitted through the grating light temporal dependence enables measurement of the in-plane component magnitude and direction, h_τ and φ_τ respectively at 7ω, 5ω frequencies, while 3ω, 9ω components are responsible for the out-of-plane h_z component of the measured magnetic field, correspondingly. Although this method allows one to determine the measured field **h,** its sensitivity is obviously much smaller than the sensitivity of the Faraday method: equation (11) implies that in the considered configuration of the magnetic field the angle associated with the measured magnetic field is multiplied by the θ_{H} which is intrinsically small.

Recent studies [10, 32, 33] show that the sensitivity of the MO magnetometers is limited mainly by the optical noise. Actually, the sensitivity of the sensor defined as the minimal registered value of the magnetic field $h_{\min}$ is determined by the following equation:

$$\frac{h_{\min}}{\sqrt{\Delta f}} = \frac{2AH}{K\Phi_0\sqrt{T}}\sqrt{2\frac{\hbar\omega_\lambda}{\mu P}}, \tag{15}$$

where Δf is the spectral bandwidth of the sensor, μ is the quantum yield of the photodetector, P is the power of the incident light, $\hbar\omega_\lambda$ is the energy of photons of incident radiation. Analysis using equation (15) provides sensitivity for the Faraday effect-based sensor up to 100 pT $\mathrm{Hz}^{-1/2}$. Similar calculation using equations (12) and (13) for quadratic MO intensity effect shows four-order of magnitude lower value of the sensitivity. However, an advantage of quadratic effect lies in the fact that signal is observed on 7th and 9th harmonics of the magnetic field rotation frequency. It is known that the optical noise quickly decreases at frequencies over the bandwidth of the laser source. For example, an optical noise of a laser with 1 MHz bandwidth more than four orders of magnitude lower at 10 MHz frequency. It means that application of narrow band laser and increasing of frequency of magnetic field rotation ω up to few megahertz can provide better sensitivity for quadratic MO effect with respect to the Faraday effect.

4. Conclusion

To conclude, we demonstrate that a 1D nanograting deposited on an iron garnet film with strong magnetic anisotropy is promising for MO magnetometry. The magnetic properties of such a grating enable the MO measurement of all orthogonal components of the weak magnetic field vector due to the multifold enhancement of the MO effects. Excitation of the guided modes allowed us to increase the thin-film Faraday rotation 100 times and intensity modulation 10 000 times compared to a smooth film of the same thickness. Although the achieved enhancement is associated with the lower transmittance of the structure, we show that MO FOM and signal-to-noise ratio are ten times enhanced compared to the uncoated film.

Two approaches, based on the even in the magnetization intensity MO effect and odd in the magnetization polarization (Faraday) effects were considered. It was shown that the Faraday rotation-based MO measurement scheme provides higher sensitivity up to 100 pT $Hz^{-1/2}$. This value of sensitivity is similar to that of recently reported MO magnetometers [10, 32, 33]. However, it was achieved either for non-vector magnetometers [32, 33] or for the thick magnetic films of 11 μm [10]. It is essential that in our scheme the sensitivity of the MO signal to all of the spatial components of the measured magnetic field is the same providing a convenient tool for low magnetic film measurements. Utilization of the thin films with nanopatterns instead of the bulk crystals is important for applications, since it allows a significant miniaturization of the device and better spatial resolution. For our structure the spatial resolution in the z-direction can be estimated as the thickness of magnetic film which equals 30 nm. The essential feature of our approach is that the developed magnetometer simultaneously provides high sensitivity to all three components of magnetic field, compactness, high spatial resolution together with operation at room temperature.

Data availability statement

All data that support the findings of this study are included within the article (and any supplementary files).

Acknowledgments

This work was financially supported by Russian Foundation for Basic Research, RFBR Project No. 18-29-02120. D O I, G A K, A N K and V I B are members the Interdisciplinary Scientific and Educational School of Moscow University “Photonic and Quantum technologies. Digital medicine”.

ORCID iDs

Daria O Ignatyeva https://orcid.org/0000-0002-1113-6021
Grigory A Knyazev https://orcid.org/0000-0002-7747-3119
Andrey N Kalish https://orcid.org/0000-0001-9984-9028
Alexander I Chernov https://orcid.org/0000-0002-6492-9068
Vladimir I Belotelev https://orcid.org/0000-0002-6939-4728

References

[1] Kwong J S, Leithauser B, Park J W and Yu C M 2013 Diagnostic value of magnetocardiography in coronary artery disease and cardiac arrhythmias: a review of clinical data *Int. J. Cardiol.* **167** 1835–42
[2] Shiono J, Horigome H, Matsui A, Terada Y, Miyashita T and Tsukada K 2003 Detection of repolarization abnormalities in patients with cardiomyopathy using current vector mapping technique on magnetocardiogram *Int. J. Cardiovasc. Imaging* **19** 163–70
[3] Baillet S 2017 Magnetoencephalography for brain electrophysiology and imaging *Nat. Neurosci.* **20** 327
[4] Espy M, Flynn M, Gomez J, Hanson C, Kraus R, Magnelind P and Peters M 2010 Ultra-low-field MRI for the detection of liquid explosives *Supercond. Sci. Technol.* **23** 034023
[5] Burch J L, Torbert R B, Phan T D, Chen L J, Moore T E, Ergun R E and Wang S 2016 Electron-scale measurements of magnetic reconnection in space *Science* **352** aaf2939
[6] Primdahl F 1979 The fluxgate magnetometer *J. Phys. E: Sci. Instrum.* **12** 241
[7] Vázquez M, Knobel M, Sánchez M L, Valenzuela R and Zhukov A P 1997 Giant magnetoimpedance effect in soft magnetic wires for sensor applications *Sens. Actuators* A **59** 20–29
[8] Korepanov V and Marusenkov A 2012 Flux-gate magnetometers design peculiarities *Surv. Geophys.* **33** 1059–79
[9] Vetoshko P M, Gusev N A, Chepurnova D A, Samoilova E V, Syvorotka I I, Syvorotka I M, Zvezdin A K, Korotaeva A A and Belotelov V I 2016 Flux-gate magnetic field sensor based on yttrium iron garnet films for magnetocardiography investigations *Tech. Phys. Lett.* **42** 860–4
[10] Rogachev A E *et al* 2016 Vector magneto-optical sensor based on transparent magnetic films with cubic crystallographic symmetry *Appl. Phys. Lett.* **109** 162403
[11] Višňovský Š, Lišková-Jakubisová E, Harward I and Celinski Z 2018 Vector MO magnetometry for mapping microwave currents *AIP Adv.* **8** 056642
[12] Arakelyan S, Galstyan O, Lee H, Babajanyan A, Lee J H, Friedman B and Lee K 2016 Direct current imaging using a magneto-optical sensor *Sens. Actuators* A **238** 397–401
[13] Goto T, Dorofeenko A V, Merzlikin A M, Baryshev A V, Vinogradov A P, Inoue M, Lisyansky A A and Granovsky A B 2008 Optical Tamm states in one-dimensional magnetophotonic structures *Phys. Rev. Lett.* **101** 113902
[14] Kahl S and Grishin A M 2005 Magneto-optical rotation of a one-dimensional all-garnet photonic crystal in transmission and reflection *Phys. Rev.* B **71** 205110
[15] Musorin A I, Sharipova M I, Dolgova T V, Inoue M and Fedyanin A A 2016 Ultrafast Faraday rotation of slow light *Phys. Rev. Appl.* **6** 024012
[16] Borovkova O V, Ignatyeva D O, Sekatskii S K, Karabchevsky A and Belotelov V I 2020 High-Q surface electromagnetic wave resonance excitation in magnetophotonic crystals for supersensitive detection of weak light absorption in the near-infrared *Photon. Res.* **8** 57–64
[17] Lodewijks K, Maccaferri N, Pakizeh T, Dumas R K, Zubritskaya I, Åkerman J, Vavassori P and Dmitriev A 2014 Magnetoplasmonic design rules for active magneto-optics *Nano Lett.* **14** 7207–14
[18] Caballero B, García-Martín A and Cuevas J C 2016 Hybrid magnetoplasmonic crystals boost the performance of nanohole arrays as plasmonic sensors *ACS Photonics* **3** 203–8
[19] Ignatyeva D O, Kalish A N, Levkina G Y and Sukhorukov A P 2012 Surface plasmon polaritons at gyrotropic interfaces *Phys. Rev.* A **85** 043804
[20] Li R and Levy M 2005 Bragg grating magnetic photonic crystal waveguides *Appl. Phys. Lett.* **86** 251102
[21] Royer F, Varghese B, Gamet E, Neveu S, Jourlin Y and Jamon D 2020 Enhancement of both Faraday and Kerr effects with an all-dielectric grating based on a magneto-optical nanocomposite material *ACS Omega* **5** 2886–92
[22] Voronov A A, Dolendra K, Ignatyeva D O, Kozhaev M A, Levy M and Belotelov V I 2020 Magneto-optics of subwavelength all-dielectric gratings *Opt. Express* **28** 17988–96

[23] Ignatyeva D O, Karki D, Voronov A A, Kozhaev M A, Krichevsky D M, Chernov A I, Levy M and Belotelov V I 2020 All-dielectric magnetic metasurface for advanced light control in dual polarizations combined with high-Q resonances *Nat. Commun.* **11** 1–8
[24] Sawicki M, Stefanowicz W and Ney A 2011 Sensitive SQUID magnetometry for studying nanomagnetism *Semicond. Sci. Technol.* **26** 064006
[25] Kittmann A *et al* 2018 Wide band low noise love wave magnetic field sensor system *Sci. Rep.* **8** 278
[26] Yahata K, Matsuzaki Y, Saito S, Watanabe H and Ishi-Hayase J 2019 Demonstration of vector magnetic field sensing by simultaneous control of nitrogen-vacancy centers in diamond using multi-frequency microwave pulses *Appl. Phys. Lett.* **114** 022404
[27] Roy A, Sampathkumar P and Anil Kumar P S 2020 Development of a very high sensitivity magnetic field sensor based on planar Hall effect *Measurement* **156** 107590
[28] Wei F, Mallik A K, Liu D, Wu Q, Peng G-D, Farrell G and Semenova Y 2017 Magnetic field sensor based on a combination of a microfiber coupler covered with magnetic fluid and a Sagnac loop *Sci. Rep.* **7** 4725
[29] Syvorotka I I, Vetoshko P M, Skidanov V A, Shavrov V G and Syvorotka I M 2015 In-plane transverse susceptibility of (111)-oriented iron garnet films *IEEE Trans. Magn.* **51** 2000703
[30] Chernov A I, Kozhaev M A, Ignatyeva D O, Beginin E N, Sadovnikov A V, Voronov A A, Karki D, Levy M and Belotelov V I 2020 All-dielectric nanophotonics enables tunable excitation of the exchange spin waves *Nano Lett.* **20** 5259–66
[31] Zvezdin A K and Kotov V A 1997 *Modern Magnetooptics and Magnetooptical Materials* (Boca Raton, FL: CRC Press)
[32] Knyazev G A *et al* 2018 Magnetoplasmonic crystals for highly sensitive magnetometry *ACS Photonics* **5** 4951–9
[33] Belyaev V K, Rodionova V V, Grunin A A, Inoue M and Fedyanin A A 2020 Magnetic field sensor based on magnetoplasmonic crystal *Sci. Rep.* **10**7133